

Article | Received 23 March 2025; Accepted 28 April 2025; Published 7 May 2025
<https://doi.org/10.55092/bm20250009>

Titanium-protoporphyrin IX coordinated nanoparticles for tumor photodynamic and sonodynamic combination therapy

Wei Wang^{1,†}, Yong Li^{2,†}, Yan Li¹, Yuzi Huang¹, Peng Geng^{1,2,*}, Liu Huang³, Youfang Zhang⁴, Wenquan Huang^{2,*} and Shuzhang Xiao^{1,*}

¹ College of Materials and Chemical Engineering, China Three Gorges University, Yichang 443000, China

² College of Medicine and Health Science, China Three Gorges University, Yichang 443000, China

³ College of Basic Medical Science, China Three Gorges University, Yichang 443000, China

⁴ Hubei Key Laboratory of Polymer Materials, Ministry of Education Key Laboratory for Green Preparation and Application of Functional Materials, School of Materials Science and Engineering, Hubei University, Wuhan 430062, China

† Joint first authors.

* Correspondence author(s); E-mail(s): gengpeng@ctgu.edu.cn (P.G.); huangwenquan@ctgu.edu.cn (W.H.); shuzhangxiao@ctgu.edu.cn (S.X.).

Highlights:

- A new photo-sonosensitizer was synthesized by coordinating Ti^{4+} with PpIX.
- TiPPs exhibit high ROS generation ability.
- TiPPs achieved good PDT-SDT combination therapy for tumor model.

Abstract: Driven by advancements in nanotechnology and biomedicine, multifunctional nanomaterials integrating photodynamic therapy (PDT) and sonodynamic therapy (SDT) are paving new avenues for efficient tumor treatment. In this study, titanium-protoporphyrin coordinated nanoparticles (TiPPs) with a uniform particle size (~70 nm) were successfully fabricated via coordination self-assembly, achieved through the rational selection of a biocompatible metal and functionalized organic ligand. Experimental results demonstrated that after 6 minutes of light or ultrasound irradiation, TiPPs exhibited high reactive oxygen species (ROS) generation efficiency, with DPBF oxidation rates of 71.6% (light group) and 46.6% (ultrasound group), confirming their excellent photo- and sono-responsive ROS production capabilities. Notably, *in vitro* cytotoxicity assays and *in vivo* tumor-bearing mouse model studies revealed that the PDT-SDT combination therapy achieved significantly higher tumor inhibition rates than single-mode treatments. This study not only establishes an efficient dual-modal synergistic therapeutic platform but also introduces an innovative paradigm for the development of multifunctional sensitizers through metal-organic coordination engineering, highlighting promising clinical applications.



Copyright©2025 by the authors. Published by ELSP. This work is licensed under Creative Commons Attribution 4.0 International License, which permits unrestricted use, distribution, and reproduction in any medium provided the original work is properly cited.

Keywords: photodynamic therapy; sonodynamic therapy; Protoporphyrin IX (PpIX); metal-organic coordinated nanoparticles; reactive oxygen species (ROS)

1. Introduction

In recent years, emerging nanotechnology-based therapeutic strategies have revolutionized the field of precision oncology [1,2]. Among them, photodynamic therapy (PDT) and sonodynamic therapy (SDT) have garnered significant attention due to their non-invasive nature [3,4]. PDT relies on photosensitizers activated by light at specific wavelengths to generate cytotoxic reactive oxygen species (ROS) [5,6]. However, its therapeutic efficacy is limited by the shallow tissue penetration of light (< 1 cm), making it less effective for treating deep-seated tumors [7,8]. In contrast, SDT employs ultrasound (US) to activate sonosensitizers, generating ROS with a much deeper tissue penetration of over 10 cm while avoiding ionizing radiation risks [9,10]. However, SDT generally exhibits a lower ROS yield compared to PDT. To overcome these limitations, a PDT-SDT combination therapy has been proposed, leveraging multimodal energy activation to enhance ROS production while addressing the depth limitations of individual treatments [11,12]. The key to this approach lies in the development of novel nanomaterials with dual photo-sonosensitizing capabilities.

Existing sensitizers suffer from significant limitations. Organic small-molecule sensitizers (e.g., hematoporphyrin and protoporphyrin) have poor hydrophilicity, rapid metabolism, and a tendency to aggregate *in vivo* [13,14]. These properties hinder their tumor-targeting efficiency and lead to fluorescence quenching, reducing their therapeutic effectiveness. Inorganic nanosensitizers (e.g., TiO₂ and Cu-WO_{3-x}) often exhibit low ROS generation efficiency due to rapid electron-hole recombination, and their poor biodegradability raises concerns about potential long-term toxicity [15,16]. Therefore, it is imperative to develop new sensitizers with high ROS production efficiency, rapid biodegradability, good hydrophilicity, and imaging capabilities [17–19].

Metal-organic coordinated nanomaterials have gained widespread attention in biomedical research due to their tunable size, morphology, and ease of functionalization [20,21]. These materials can integrate metal ions as coordination nodes with organic photo-/sonosensitizers [22,23] as bridging ligands. Upon degradation, metal ions are rapidly excreted, while organic ligands contribute to controlled photo-sonodynamic therapeutic effects [24]. Several metal-organic coordinated nanomaterials with PDT potential have shown promising results in cancer treatment, including zirconium-porphyrin [3], copper-porphyrin [25,26], and iron-porphyrin [13,27] complexes. However, research on metal-organic coordinated nanomaterials as dual-mode PDT-SDT sensitizers remains scarce.

Titanium (Ti), known for its excellent biocompatibility, has been widely used in orthopedic implants and dental materials [18,28,29]. Its low cytotoxicity, corrosion resistance, and excretion clearance make it a promising candidate for *in vivo* applications. Meanwhile, protoporphyrin IX (PpIX) [30–32], an FDA-approved clinical photosensitizer, has demonstrated outstanding safety in both PDT and SDT applications. In this study, we designed and synthesized titanium-protoporphyrin coordinated nanoparticles [33] (TiPPs, Figure 1(a)) via coordination self-assembly, integrating the safety features of both components while achieving spatiotemporally controlled ROS generation through a photo-sonodynamic synergy. Experimental results demonstrated that under 660 nm light and ultrasound irradiation, TiPPs achieved DPBF degradation rates of 71.6% and 46.6%, respectively, within six minutes. Both *in vitro* and *in vivo* studies revealed that the combination therapy (660 nm Light + US)

significantly outperformed single-mode PDT or SDT treatments. These findings confirm the potent photo-sonodynamic therapeutic potential of TiPPs (Figure 1(b)).

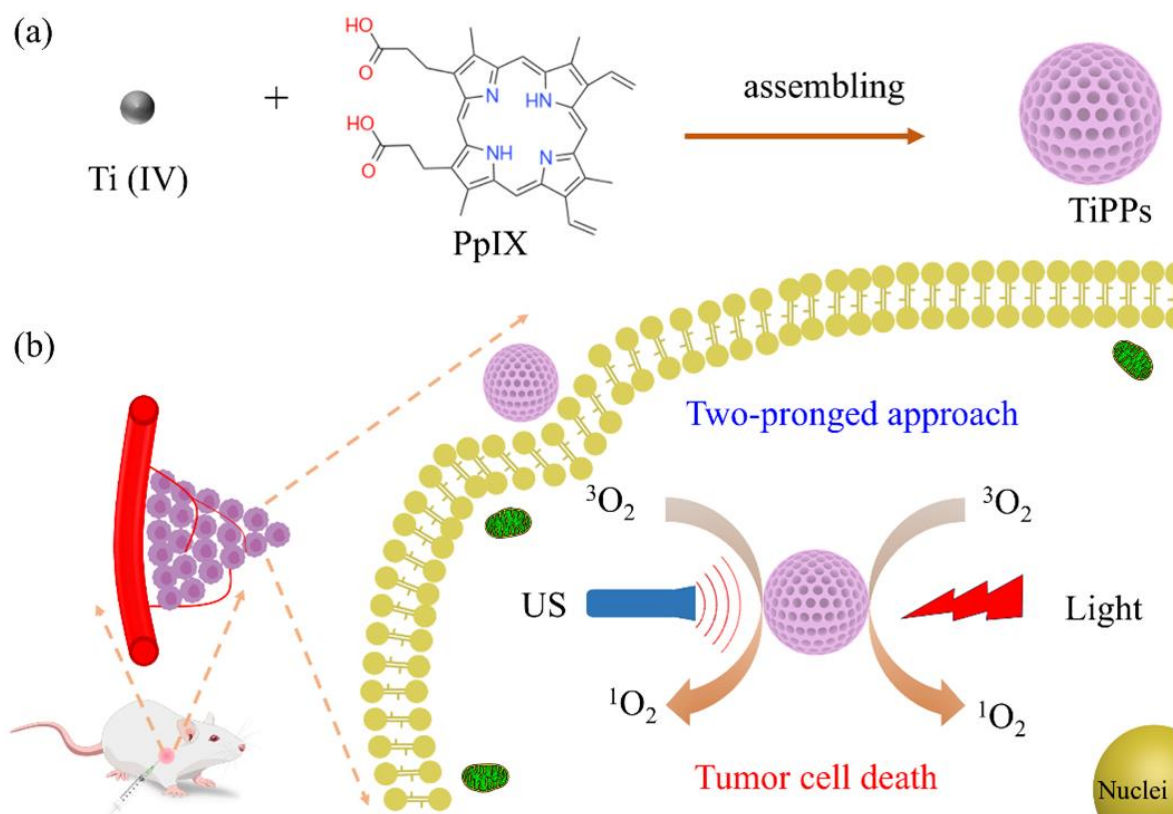


Figure 1. Schematic diagram of material preparation and tumor treatment mechanism. (a) Schematic illustration of the synthesis of TiPPs and (b) the mechanism of tumor photodynamic-sonodynamic (PDT-SDT) combination therapy.

2. Methods

2.1. Synthesis, characterization, and performance evaluation of TiPPs

Synthesis of TiPPs: To prepare TiPPs, 2 mg of protoporphyrin IX (PpIX) and 5 mg of polyvinylpyrrolidone (PVP) were dispersed in a mixed solvent containing triethylamine (0.5 mL) and *N,N*-dimethylformamide (DMF, 15 mL). The solution was stirred under a nitrogen atmosphere for 10 min. Subsequently, the mixture was transferred to a 25 mL reaction vessel, followed by the addition of 10 μL of titanium tetrachloride (TiCl_4) solution. The reaction was carried out at 110 $^\circ\text{C}$ under nitrogen protection for 4 h. After naturally cooling to room temperature, the resulting product was sequentially washed three times with anhydrous ethanol and deionized water via centrifugation, yielding the TiPPs nanoparticles. Finally, the TiPPs nanoparticles were dried, weighed, and then dispersed to the desired concentration for use.

2.2. Singlet oxygen ($^1\text{O}_2$) detection

To evaluate singlet oxygen ($^1\text{O}_2$) generation, a 2.0 mg/mL DPBF-DMF solution and a 40 $\mu\text{g/mL}$ TiPPs-DMF solution were prepared. A total of 3 mL of the TiPPs-DMF solution was mixed with 20 μL of the DPBF-DMF solution, followed by the following treatments: (a) 660 nm laser irradiation (100 mW/cm^2 ;

(b) Ultrasound irradiation (1.0 MHz, 1.5 W/cm²). During the experiment, air was intermittently bubbled into the solution for 30 s every minute, for a total duration of 6 min. To compare the singlet oxygen generation efficiency, control groups were tested under the same conditions: TiPPs + Light, DPBF + Light, TiPPs + US, and DPBF + US. The efficiency of ¹O₂ production was assessed by monitoring the absorbance changes at 415 nm.

2.3. Cytotoxicity assessment

The cytotoxicity of TiPPs was evaluated using 4T1 murine breast cancer cells and L929 murine fibroblast cells. Cells were seeded into 96-well plates (~1 × 10⁴ cells per well) and incubated for 24 h, after which fresh DMEM medium containing TiPPs (0~400 µg/mL) was added. After an additional incubation period of 24 or 48 h, cells were washed with PBS, and viability was determined using the MTT assay.

2.4. *In vitro* therapeutic evaluation

For *in vitro* therapy assessment, 4T1 cells were incubated with 100 µg/mL TiPPs for 5 h, followed by: (a) photodynamic therapy (660 nm, 100 mW/cm²); (b) sonodynamic therapy (1.0 MHz, 1.5 W/cm²); (c) combined PDT-SDT therapy. Each treatment was applied for 3, 5, or 10 min, and cell viability at different time points was measured using the MTT assay.

2.5. *In vivo* antitumor study

To assess the therapeutic efficacy of TiPPs *in vivo*, 4T1 tumor-bearing mice were randomly divided into five groups (n = 4): (a) PBS control group: 80 µL PBS; (b) TiPPs group: 80 µL TiPPs (1.0 mg/mL); (c) TiPPs + PDT group: TiPPs with 10 min light irradiation; (d) TiPPs + SDT group: TiPPs with 10 min ultrasound irradiation; (e) TiPPs + Combination therapy group: TiPPs with 10 min light and 10 min ultrasound irradiation. Four hours after intratumoral injection, each group received its respective treatment. Tumor volume was calculated using the formula $V = L \times W^2/2$ (where L is the tumor length and W is the width). The therapeutic effect was evaluated by tracking the relative tumor volume (V/V_0 , where V_0 is the initial tumor volume).

3. Results

3.1. Coordination structure characterization of TiPPs

Titanium-protoporphyrin IX coordinated nanoparticles (TiPPs) were successfully synthesized via a self-assembly approach. To characterize their morphology and physicochemical properties, scanning electron microscopy (SEM), dynamic light scattering (DLS), and zeta potential analysis were conducted. SEM images and particle size distribution analysis (Figure 2(a, b)) revealed that TiPPs exhibited a near-spherical structure with a dry-state particle size of approximately 70 nm. However, the DLS measurements (Figure 2(c)) indicate that the hydrated particle sizes are 180 nm in deionized water (PDI = 0.10) and 220 nm in PBS solution (PDI = 0.11), which are significantly larger than the size of the dry particles. This difference arises because DLS measures the size of the solvent layer surrounding the nanoparticles, along with the movement of associated molecules (e.g., PVP), whereas SEM only

measures the core size of the dried particles. The UV absorption of TiPPs in PBS solution remained nearly unchanged after 3 days (Figure S1), indicating that the material exhibited good stability in biological fluids. Furthermore, zeta potential analysis (Figure 2(d)) demonstrated a notable shift in surface charge. The zeta potential of PpIX was measured at -20.9 mV, whereas TiPPs exhibited an increased potential of -14.7 mV. This change suggests that Ti^{4+} effectively modulated the surface electrostatic potential of PpIX through charge neutralization.

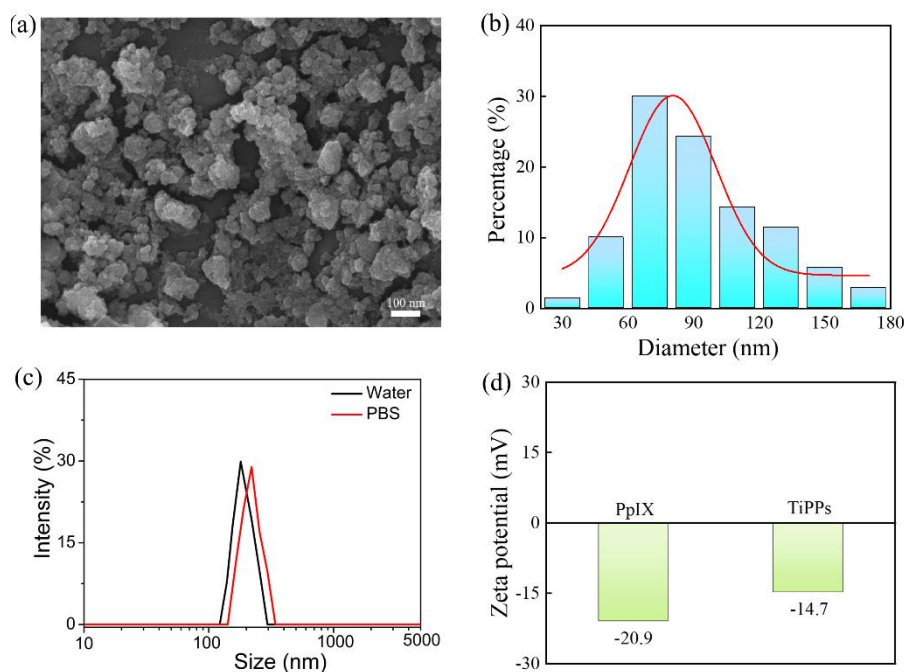


Figure 2. Morphology and size analysis of TiPPs. **(a, b)** Scanning electron microscopy (SEM) images and particle size distribution of TiPPs; **(c)** hydrodynamic diameter distribution of TiPPs; **(d)** Zeta potential analysis.

The coordination structure of TiPPs was systematically characterized using X-ray photoelectron spectroscopy (XPS), Fourier-transform infrared spectroscopy (FT-IR), ultraviolet-visible (UV-vis) absorption spectroscopy, and fluorescence (FL) spectroscopy. The full XPS spectrum (Figure 3(a)) revealed a distinct Ti 2p characteristic peak in TiPPs, while the C 1s, N 1s, and O 1s peaks remained consistent with those of PpIX, confirming that the titanium component originated from the TiCl_4 precursor and the organic moiety was inherited from PpIX. High-resolution XPS spectra provided further insights: the Ti 2p orbital exhibited a characteristic doublet at 458.4 eV and 464 eV (Figure 3(b)), corresponding to the Ti^{4+} $2p_{3/2}$ and $2p_{1/2}$ states, respectively. Additionally, a new binding energy peak appeared at 530.1 eV in the O 1s spectrum (Figure 3(c)), confirming the formation of Ti-O coordination bonds. Notably, the N 1s and C 1s spectra (Figure S2(a, b)) showed no significant shifts, indicating that the porphyrin core was not directly involved in coordination. FT-IR spectroscopy further validated the coordination mechanism. Compared to PpIX, the characteristic carboxyl peak at 1705 cm^{-1} disappeared in TiPPs, while two new peaks emerged at 1643 cm^{-1} (asymmetric stretching vibration) and 1417 cm^{-1} (symmetric stretching vibration) (Figure 3(d)), confirming the deprotonation and coordination of carboxyl groups with Ti^{4+} . The UV-vis spectrum (Figure 3(e)) demonstrated that TiPPs retained the characteristic Soret band of PpIX at 410 nm, along with four Q-bands at 505, 539, 575, and 627 nm. The

presence of four distinct Q-bands ruled out the possibility of metal coordination at the porphyrin core. FL spectroscopy further supported this conclusion, showing that under 560 nm excitation, the fluorescence emission intensity of TiPPs at 632 nm was significantly quenched compared to PpIX (Figure 3(f)). This fluorescence quenching effect was attributed to energy transfer induced by the coordination of Ti^{4+} . Collectively, these results confirm that Ti^{4+} selectively coordinates with the carboxyl groups of PpIX, driving the self-assembly of nanoparticles via metal-organic coordination (Figure S3) while effectively preserving the intrinsic photophysical properties of the porphyrin ring.

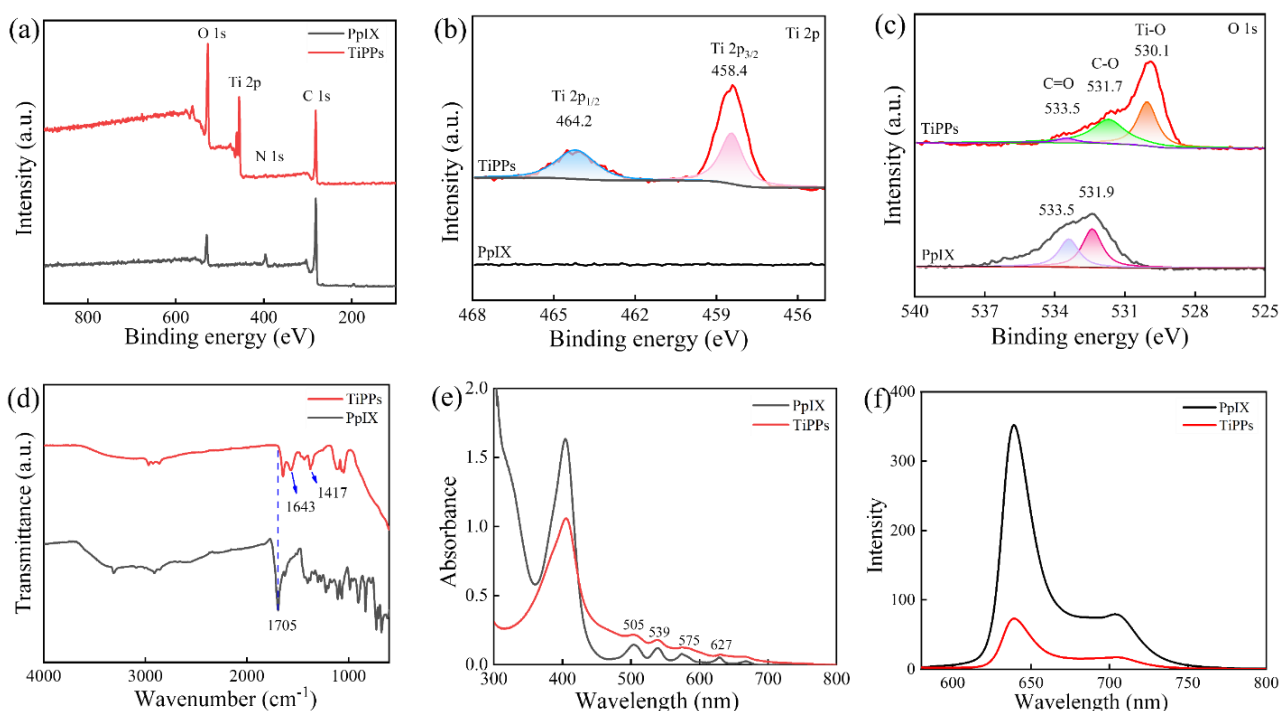


Figure 3. The structural analysis of TiPPs. **(a)** XPS spectrum of TiPPs; **(b)** high-resolution Ti 2p spectrum; **(c)** O 1s spectrum; **(d)** FTIR spectra of PpIX and TiPPs; **(e)** UV-vis absorption spectra; **(f)** fluorescence spectra of TiPPs.

3.2. Investigation of ROS generation by light/ultrasound-responsive TiPPs

TiPPs incorporate the photo-/sonosensitizer PpIX, which can convert oxygen into cytotoxic singlet oxygen (1O_2) upon activation by light or US (Figure 4(a)). To quantitatively assess 1O_2 generation efficiency, we employed the selective probe DPBF, which undergoes a specific reaction with 1O_2 , leading to a decrease in its characteristic absorption peak at 410 nm. Experimental results demonstrated that after 6 min of 660 nm laser irradiation (100 mW/cm²), DPBF absorbance decreased by 71.6% (Figure 4(b)). Under ultrasound irradiation at 1.0 MHz (1.5 W/cm²) for the same duration, the absorbance reduction reached 46.6% (Figure 4(c)). To systematically verify the ROS generation capability of TiPPs (Figure 4(d)), additional control groups were included: a TiPPs dispersion without DPBF and a pure DPBF solution without TiPPs. As shown in Supporting Information (Figure S4, S5 and S6), neither control group exhibited significant absorbance changes under identical light/US irradiation conditions. These findings suggest that TiPPs can effectively generate 1O_2 under light or US activation, and under

the same conditions, they show better $^1\text{O}_2$ generation performance than the previously reported Mn-PpIX nanocomposites [12], making them a promising candidate for ROS-based therapeutic applications.

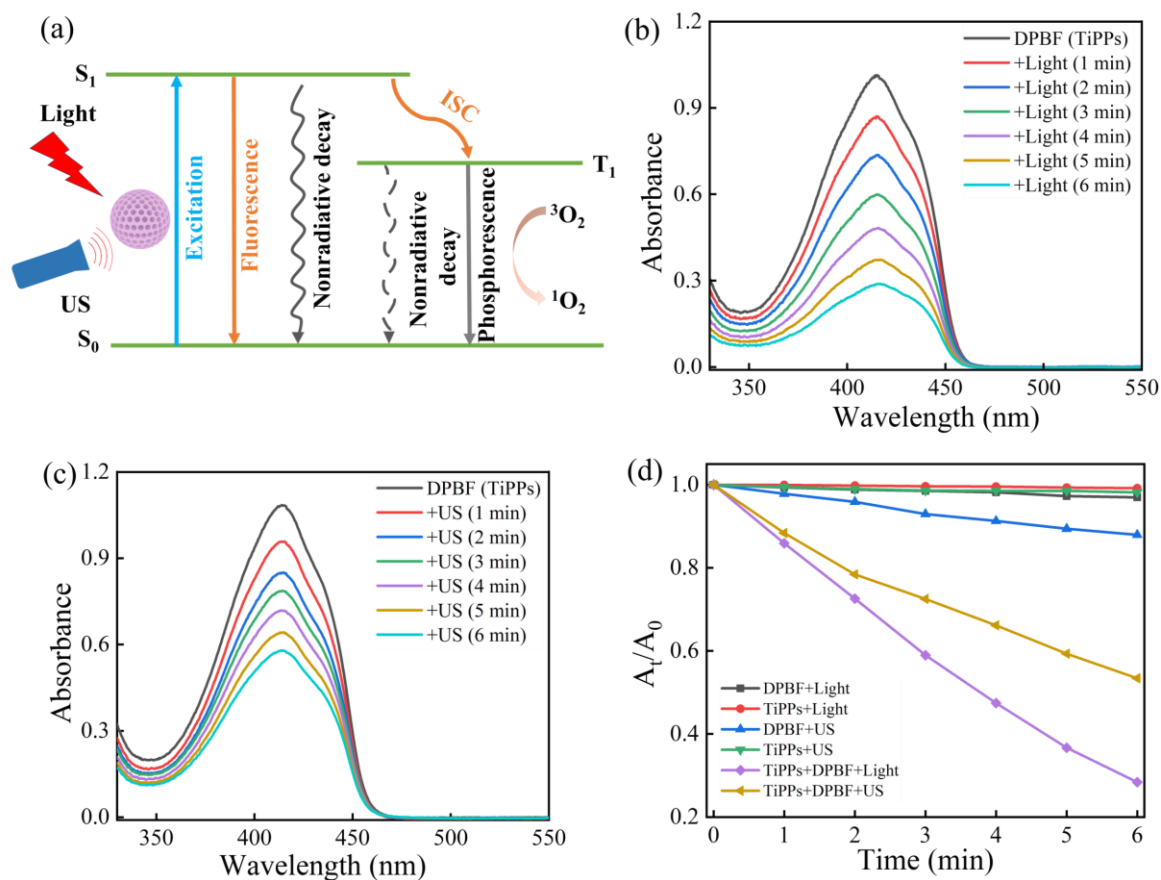


Figure 4. Investigation of ROS generation by light/US-responsive TiPPs. (a) Schematic illustration of $^1\text{O}_2$ generation by TiPPs upon light/US activation; (b) time-dependent absorption spectra of DPBF solution during TiPPs reaction under light irradiation and (c) US exposure; (d) oxidation performance of DPBF under different conditions.

3.3. *In vitro* cell experiments

Biocompatibility is a fundamental prerequisite for the biomedical application of nanomaterials. In this study, murine breast cancer cells (4T1) were selected as the tumor model, while murine fibroblast cells (L929) were used as the normal cell model to systematically evaluate the cytocompatibility of TiPPs. Cell viability was assessed using the standard MTT colorimetric assay. Results showed a clear time-dependent effect within the tested TiPPs concentration range (0~400 $\mu\text{g}/\text{mL}$). In the normal cell model, L929 cells exhibited viability rates of 91.3% and 80.4% after 24 and 48 h of treatment with 400 $\mu\text{g}/\text{mL}$ TiPPs, respectively (Figure 5(a, b)). Similarly, for the tumor cell model, 4T1 cells treated with the same concentration of TiPPs maintained viability rates of 93.2% (24 h) and 81.3% (48 h) (Figure 5(c, d)). Notably, cell viability in both models remained above 80% even at the highest tested concentration, demonstrating the excellent biocompatibility of TiPPs within this concentration range ($\leq 400 \mu\text{g}/\text{mL}$). Based on these findings, we conclude that TiPPs exhibit a favorable safety profile and are suitable for further *in vitro* and *in vivo* therapeutic studies at concentrations up to 400 $\mu\text{g}/\text{mL}$.

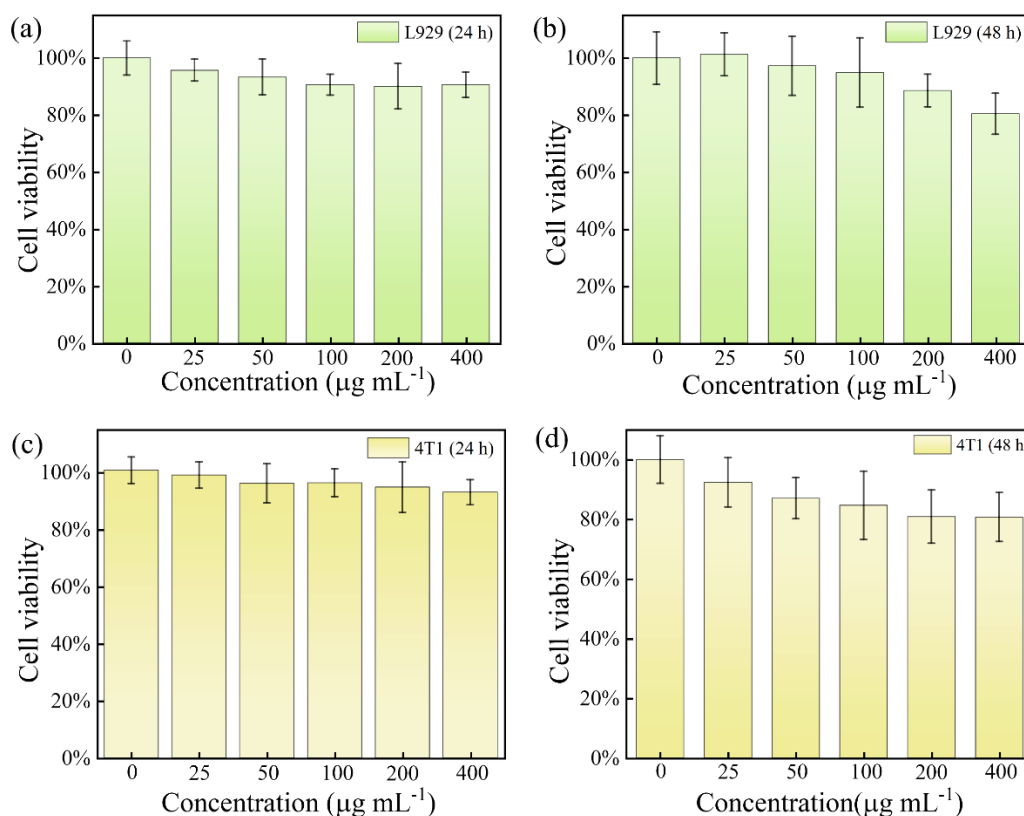


Figure 5. The biocompatibility of TiPPs. (a, b) Cytotoxicity of TiPPs on L929 cells after 24 and 48 h of treatment; (c, d) cytotoxicity of TiPPs on 4T1 cells after 24 and 48 h of treatment ($n = 3$).

3.4. Evaluation of *in vitro* photodynamic-sonodynamic combination therapy with TiPPs

The *in vitro* therapeutic efficacy of TiPPs in PDT-SDT combination therapy was systematically assessed. The generation of ROS in 4T1 cells incubated with TiPPs (100 µg/mL) for 5 h was measured using the DCFH-DA probe. As shown in (Figure 6(a)), both the control group and the TiPPs-only group exhibited weak fluorescence signals, indicating minimal ROS production in the absence of external stimulation. In contrast, the fluorescence intensity significantly increased in the PDT group (660 nm laser, 100 mW/cm²) and the SDT group (1.0 MHz ultrasound, 1.5 W/cm²), confirming that either physical stimulus alone effectively activated TiPPs to generate ROS. Notably, the fluorescence signal in the combination therapy group was even stronger than in the single-treatment groups, highlighting the enhanced ROS generation efficiency due to the synergistic effect of PDT and SDT. MTT assay results further quantified the cytotoxicity of different treatment conditions. In the PDT treatment group, the TiPPs-only group maintained a high cell viability of over 98.5%, showing almost no difference from the Control group and demonstrating excellent biocompatibility. As the irradiation time increased from 3 minutes to 10 minutes, the cell viability showed a time-dependent attitude, decreasing from 87.3% to 24.4% (Figure 6(b)). In the SDT treatment group, the TiPPs-only group maintained 97.4% of the cell viability. Similarly, the SDT group showed a time-dependent cytotoxic effect, reducing cell viability to 55.5% after 10 minutes of ultrasound exposure (Figure 6(c)). Strikingly, the combination therapy group experienced a dramatic drop in viability to 16.1% under the same treatment duration (10 min), significantly lower than either single-treatment group, indicating a pronounced synergistic effect (Figure 6(d)). In addition, the IC₅₀

values of TiPPs for PDT, SDT, and PDT-SDT in the treatment of 4T1 cells are 6.5, 10.6, and 4.8 minutes, respectively, indicating that the PDT-SDT combination therapy achieves the same therapeutic effect in the shortest time (Figure S7). Live/dead cell staining using Calcein-AM/PI further validated these findings. In the combination therapy group, red fluorescence (indicative of dead cells) dominated the entire field of view, whereas the single PDT or SDT groups still showed some residual green fluorescence (indicative of live cells, Figure 6(e)). These results strongly demonstrate that TiPPs exhibit excellent dual photo-sonodynamic responsiveness, and the combination therapy strategy significantly enhances therapeutic efficacy.

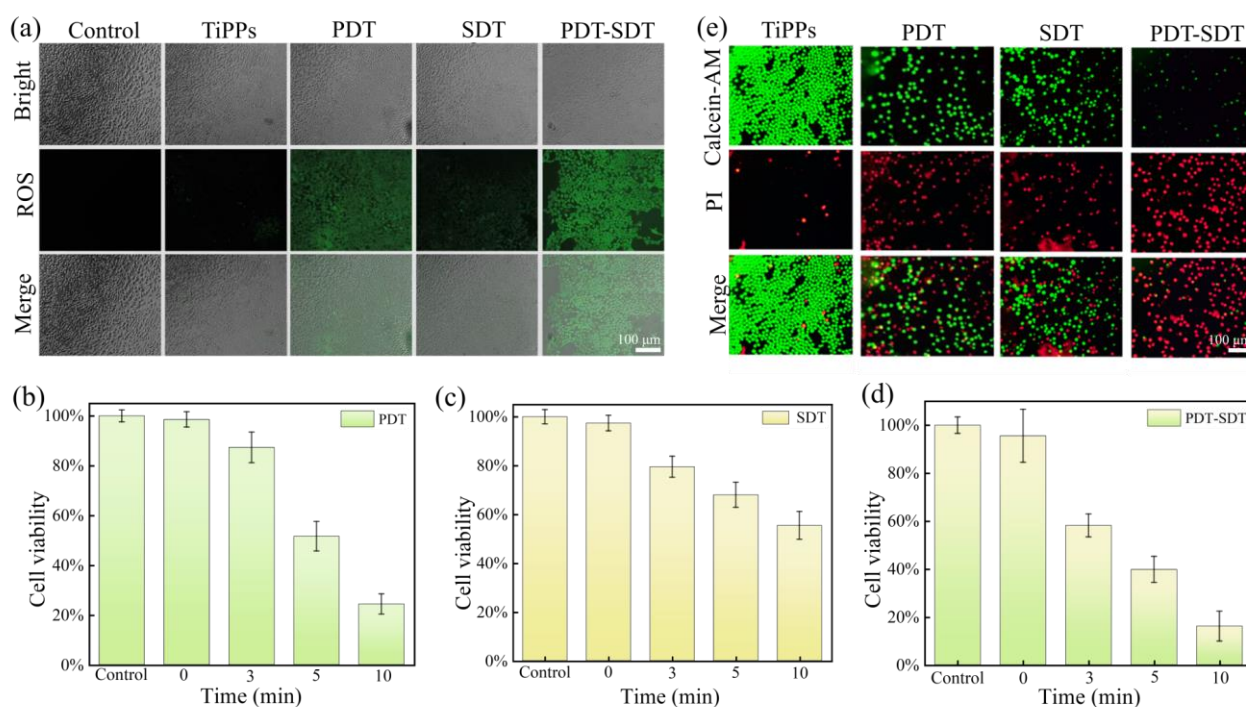


Figure 6. Evaluation of *in vitro* PDT and/or SDT with TiPPs. (a) Fluorescence images of ROS staining in 4T1 cells after different treatments; cell viability at various treatment durations ($n = 3$) for PDT (b), SDT (c), and PDT-SDT combination therapy (d); (e) live/dead fluorescence staining images of 4T1 cells following different treatments.

3.5. *In vivo* antitumor study

In view of the favorable effect of TiPPs on PDT-SDT *in vitro*, we further evaluated the antitumor effect of TiPPs *in vivo* in a 4T1 tumor-bearing mouse model (Figure 7(a)). In this study, 4T1 tumor-bearing mice were randomly divided into five groups ($n = 4$): (1) Control group: Saline (80 μL); (2) TiPPs-only group: TiPPs (80 μL, 1.0 mg/mL); (3) PDT group: TiPPs (80 μL, 1.0 mg/mL) + Light (660 nm, 10 min); (4) SDT group: TiPPs (80 μL, 1.0 mg/mL) + US (1.5 W/cm², 10 min); (5) PDT-SDT combination group: TiPPs (80 μL, 1.0 mg/mL) + Light (660 nm, 10 min) + US (1.5 W/cm², 10 min). After 12 days of treatment, no significant differences in body weight were observed among the groups, indicating that all treatment methods exhibited low systemic toxicity (Figure 7(b)). As expected, due to the lack of therapeutic effects in the saline and TiPPs-only groups, tumors in groups (1) and (2) grew rapidly, reaching 4.2 and 3.4 times their initial volumes, respectively. Compared to these control groups, PDT

(group 3) and SDT (group 4) treatments alone demonstrated limited tumor suppression, with tumor volumes reaching 2.6 and 2.1 times the initial size, respectively. The slightly better therapeutic effect of SDT over PDT may be attributed to the superior tissue penetration and utilization of US compared to light. Notably, the PDT-SDT combination therapy group (group 5) exhibited the most significant tumor inhibition, with tumor volume only increasing 1.4 times from the initial size, demonstrating the superior therapeutic efficacy of the synergistic PDT-SDT effect (Figure 7(c)). Further validation came from tumor mass measurements (Figure 7(d)) and tumor photographs (Figure 7(e)), both of which showed that group 5 had the smallest tumor size and weight among all groups. Moreover, for TiPPs + Light group, TiPPs + US group and TiPPs + Light + US group, tumor cells were found with the condensed nuclei and the unclear cell morphology, whereas the structure of tumor cells were barely affected for other groups, as proved by the typical images of hematoxylin and eosin (H&E)-stained tumor slices (Figure 7(f)). Overall, these results confirm that TiPPs exhibit excellent *in vivo* PDT-SDT combined antitumor efficacy, highlighting their potential for advanced cancer therapy.

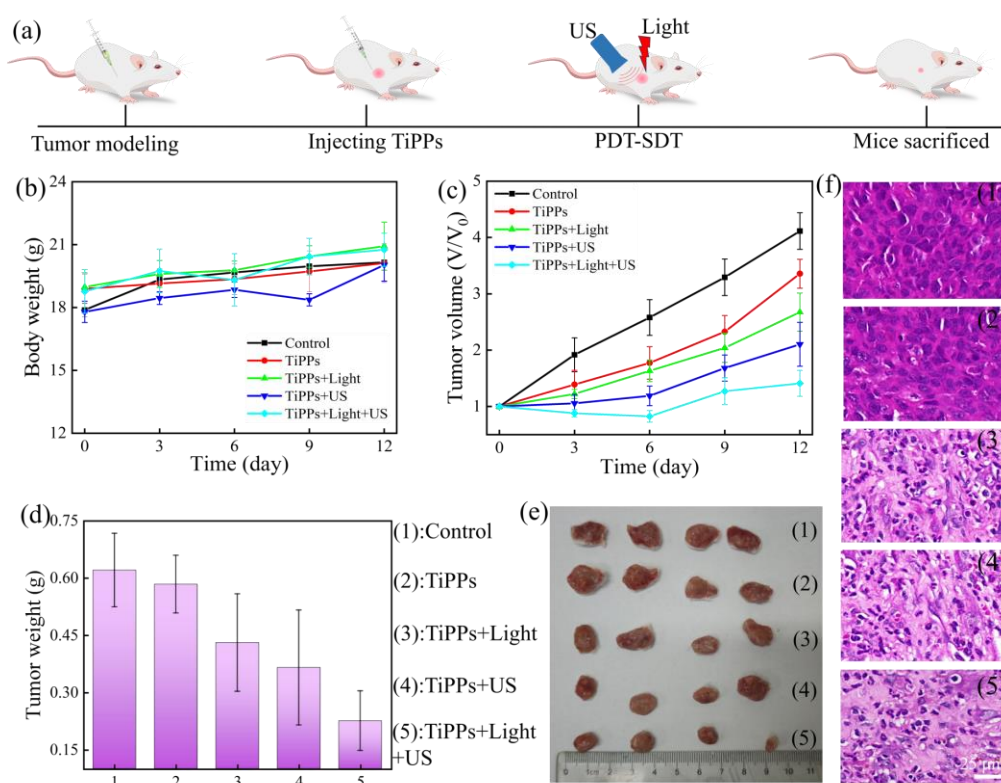


Figure 7. Evaluation of *in vivo* PDT and/or SDT with TiPPs. (a) Schematic illustration of the *in vivo* treatment process; (b) body weight changes of mice during treatment; (c) relative tumor volume in different treatment groups; (d) tumor mass measurements; (e) representative images of excised tumors from each group; (f) the photograph and representative images of H&E-stained tumor slices.

4. Conclusion

In this study, a nanoscale TiPPs material was successfully synthesized via a solvothermal self-assembly process involving Ti^{4+} ions and protoporphyrin IX (PpIX). Compared with existing multifunctional nanomaterials designed for synergistic photodynamic-sonodynamic therapy (PSDT), the “two-in-one” TiPPs material developed in this study offers two significant advantages: (a) Excellent biocompatibility:

The material is composed of biocompatible titanium ions and the clinically approved porphyrin-based drug PpIX, ensuring superior biosafety. (b) Dual light/ultrasound responsiveness: Through a simple one-step self-assembly process, TiPPs exhibits simultaneous responsiveness to both light and ultrasound, enabling efficient reactive oxygen species (ROS) generation under different external energy sources. This dual activation capability facilitates enhanced synergistic photodynamic-sonodynamic tumor therapy. This study provides a novel design strategy for developing multifunctional tumor therapeutics based on PpIX structural analogs, paving the way for safer and more effective cancer treatment approaches.

5. Supplementary data

The authors confirm that the supplementary data are available within this article.

Acknowledgments

This work was funded by the National Natural Science Foundation of China (22171163), the 111 Project (D20015), the Natural Science Foundation of Hubei Province (2024AFB059) and the Yichang Natural Science Research Program (A23-2-025).

Authors' contribution

Conceptualization, P.G. and S.X.; methodology, P.G. and W.H.; software, W.W., Y.L. and Y.H.; validation, P.G., W.H. and S.X.; formal analysis, W.W. and Y.L.; investigation, W.W., Y.L., Y.L., L.H., Y.Z. and Y.H.; resources, P.G. and S.X.; data curation, W.W. and Y.L.; writing—original draft preparation, W.W. and Y.L.; writing—review and editing, P.G.; supervision, P.G. and S.X.; project administration, P.G., W.H. and S.X.; funding acquisition, P.G. and S.X. All authors have read and agreed to the published version of the manuscript.

Conflicts of interests

The authors declare no conflict of interest.

Ethical statement

The study involving animal experiments, was performed under project license 2024010R (mouse work) approved by China Three Gorges University.

References

- [1] Sung H, Ferlay J, Siegel RL, Laversanne M, Soerjomataram I, *et al.* Global cancer statistics 2020: GLOBOCAN estimates of incidence and mortality worldwide for 36 cancers in 185 countries. *CA-Cancer J Clin.* 2021, 71(3):209–249.
- [2] Haidar ZS. Polymicellar-based drug delivery systems for use in nanodentistry, oral and cranio-maxillo-facial oncology. *Biofunct. Mater.* 2023, 1(1):0003.
- [3] Li Y, Wang W, Zhang YT, Xiao SZ, Lan HC, *et al.* Design and synthesis of nanoscale Zr-Porphyrin IX framework for synergistic photodynamic and sonodynamic therapy of tumors. *Acta Chim. Sin.* 2024, 82(04):443–448.

- [4] Cao X, Yan Y, Zhu X, Huang Z, Yang C, *et al.* Application of aggregation-induced emission (AIE) in the urinary system disease. *Biofunct. Mater.* 2025, 3(1):0005.
- [5] Yang L, Liu Y, Ren X, Jia R, Si L, *et al.* Microemulsion-assisted self-assembly of Indium porphyrin photosensitizers with enhanced photodynamic therapy. *ACS Nano.* 2024, 18(4):3161–3172.
- [6] Yu Z, Zhou P, Pan W, Li N, Tang B. A biomimetic nanoreactor for synergistic chemiexcited photodynamic therapy and starvation therapy against tumor metastasis. *Nat. Commun.* 2018, 9(1):5044.
- [7] Gong Y, Yuan W, Zhang P, Zheng K, Zhang Q, *et al.* A tumor targeted antifouling upconversion nanoplatform for fluorescence imaging and precise photodynamic therapy triggered by NIR laser. *Anal. Chim. Acta* 2023, 1274:341561.
- [8] Han J, Xu X, Jin F, Xu X, Fang T, *et al.* Tumor oxygenation nanoliposomes promote deep photodynamic therapy for triple-negative breast cancer. *Biomater. Sci.* 2024, 12(19):4967–4979.
- [9] Ma A, Chen H, Cui Y, Luo Z, Liang R, *et al.* Metalloporphyrin complex-based nanosonosensitizers for deep-tissue tumor theranostics by noninvasive sonodynamic therapy. *Small* 2019, 15(5):1804028.
- [10] Liang C, Xie J, Luo S, Huang C, Zhang Q, *et al.* A highly potent ruthenium(II)-sonosensitizer and sonocatalyst for *in vivo* sonotherapy. *Nat. Commun.* 2021, 12(1):5001.
- [11] Li Y, Huang L, Li X, Geng P, Xiang JJ, *et al.* From biomaterials to biotherapy: cuttlefish ink with protoporphyrin IX nanoconjugates for synergistic sonodynamic-photothermal therapy. *J. Mater. Chem. B* 2024, 12:1837–1845.
- [12] Geng P, Li Y, Macharia DK, Ren XL, Meng RR, *et al.* One stone, three birds: design and synthesis of “all-in-one” nanoscale Mn-porphyrin coordination polymers for magnetic resonance imaging-guided synergistic photodynamic-sonodynamic therapy. *J. Colloid Interface Sci.* 2024, 660:1021–1029.
- [13] Xu H, Yu N, Zhang JL, Wang ZJ, Geng P, *et al.* Biocompatible Fe-hematoporphyrin coordination nanoplatforms with efficient sonodynamic-chemo effect on deep-seated tumors. *Biomaterials* 2020, 257:120239.
- [14] Song K, Chen GB, He ZY, Shen J, Ping J, *et al.* Protoporphyrin-sensitized degradable bismuth nanoformulations for enhanced sonodynamic oncotherapy. *Acta Biomater.* 2023, 158:637–648.
- [15] Qin Q, Yang M, Shi Y, Cui H, Pan C, *et al.* Mn-doped Ti-based MOFs for magnetic resonance imaging-guided synergistic microwave thermal and microwave dynamic therapy of liver cancer. *Bioact. Mater.* 2023, 27:72–81.
- [16] Zhou Z, Wang T, Hu TT, Xu H, Cui L, *et al.* Synergistic interaction between metal single-atoms and defective WO_{3-x} nanosheets for enhanced sonodynamic cancer therapy. *Adv. Mater.* 2024, 36(23): 2311002.
- [17] Wang W, Zhang YT, Li Y, Huang YZ, Xiao SZ, *et al.* Preparation of cuttlefish ink-porphyrin nanoconjugates and its application in photodynamic-photothermal synergistic treatment of tumor cells. *Nano Med. Mater.* 2024, 4(1):1895.
- [18] Liang S, Xiao X, Bai L, Liu B, Yuan M, *et al.* Conferring Ti-Based MOFs with defects for enhanced sonodynamic cancer therapy. *Adv. Mater.* 2021, 33:2100333.
- [19] Geng P, Xiang GC, Zhang W, Lan HC, Xiao SZ. Hollow copper sulfide loaded protoporphyrin for photothermal-sonodynamic therapy of cancer cells. *Chin. J. Inorg. Chem.* 2024, 40(10):1903–1910.

- [20] Geng P, Yu N, Macharia DK, Meng RR, Qiu P, *et al.* MOF-derived CuS@Cu-MOF nanocomposites for synergistic photothermal-chemodynamic-chemo therapy. *Chem. Eng. J.* 2022, 441:135964.
- [21] Jia T, Du J, Yang J, Li Y, Ohulchanskyy TY, *et al.* Metalloporphyrin MOFs-based nanoagent enabling tumor microenvironment responsive sonodynamic therapy of intracranial glioma signaled by NIR - IIb luminescence imaging. *Adv. Funct. Mater.* 2023, 34(3):2307816.
- [22] Meng X, Sun S, Gong C, Yang J, Yang Z, *et al.* Ag-doped metal–organic frameworks’ heterostructure for sonodynamic therapy of deep-seated cancer and bacterial infection. *ACS Nano.* 2022, 17:1174–1186.
- [23] Liu S, Wen M, Huang M, Wang H, Chen ZG, *et al.* Nanoscale hematoporphrin-based frameworks for photo-sono synergistic cancer therapy via utilizing Al(III) as metal nodes rather than heavy metals. *J. Colloid Interface Sci.* 2022, 616:23–33.
- [24] Xu C, Dong J, Shi X, Rui J, Chen M, *et al.* Engineered microalgae for photo-sonodynamic synergistic therapy in breast cancer treatment. *Acta Biomater.* 2025, 193:531–544.
- [25] Wen M, Yu N, Yi ZG, Qiu P, Tao C, *et al.* On-demand phototoxicity inhibition of sensitizers and H₂S-triggered in-situ activation for precise therapy of colon cancer. *Nano Today* 2023, 50:101863.
- [26] Li B, Wang X, Chen L, Zhou Y, Dang W, *et al.* Ultrathin Cu-TCPP MOF nanosheets: a new theragnostic nanoplatform with magnetic resonance/near-infrared thermal imaging for synergistic phototherapy of cancers. *Theranostics* 2018, 8(15):4086–4096.
- [27] Hu X, Li R, Wu W, Fang K, Zhu Z, *et al.* A Fe(III)-porphyrin-oxaliplatin(IV) nanoplatform for enhanced ferroptosis and combined therapy. *J. Control. Release.* 2022, 348:660–671.
- [28] Xing J, Yang Y, Zhang W, Yan J, Qian H, *et al.* Injectable hydrogel containing TiO nanosheets for synergistic photothermal/thermodynamic therapy. *ACS Appl. Mater. Interfaces* 2023, 15(29):34436–34450.
- [29] Liu G, Zou J, Tang Q, Yang X, Zhang Y, *et al.* Surface modified Ti₃C₂ MXene nanosheets for tumor targeting photothermal/photodynamic/chemo synergistic therapy. *ACS Appl. Mater. Interfaces* 2017, 9(46):40077–40086.
- [30] Yan L, Amirshaghghi A, Huang D, Miller J, Stein JM, *et al.* Protoporphyrin IX (PpIX)-coated superparamagnetic iron oxide nanoparticle (SPION) nanoclusters for magnetic resonance imaging and photodynamic therapy. *Adv. Funct. Mater.* 2018, 28(16):1707030.
- [31] Zhao X, Cheng H, Wang Q, Nie W, Yang Y, *et al.* Regulating photosensitizer metabolism with DNAzyme-loaded nanoparticles for Amplified mitochondria-targeting photodynamic immunotherapy. *ACS Nano* 2023, 17(14):13746–13759.
- [32] Zuo L, Nie W, Yu S, Zhuang W, Wu G, *et al.* Smart tumor-cell-derived microparticles provide on-demand photosensitizer synthesis and hypoxia relief for photodynamic therapy. *Angew. Chem. Int. Ed.* 2021, 60(48):25365–25371.
- [33] Zhang M, Wei S, Huang H, Sun H, Zhang L, *et al.* Tailorable fabrication of optical active nanomaterials for bio-applications. *Biofunct. Mater.* 2024, 2(2):0007.